Climate Dynamics (2000) 16:79–91

E. R. Cook · B. M. Buckley · R. D. D'Arrigo
M. J. Peterson

Warm-season temperatures since 1600 BC reconstructed from Tasmanian tree rings and their relationship to large-scale sea surface temperature anomalies

Received: 12 January 1999 / Accepted: 31 July 1999

Abstract We describe an improved tree-ring reconstruction of mean warm-season (November–April) temperatures for Tasmania from Huon pine. This record extends back to 1600 BC and is based on a tree-ring chronology that was processed to retain as much low-frequency variance as possible. The resulting reconstruction explains 46.6% of the variance and verifies significantly when compared to withheld instrumental data. Cross-spectral analysis of actual and estimated temperatures over the 1886–1991 common period indicates that most of the unexplained variance is at periods <12 years in length. At periods >12 years, the squared coherency ranges between 0.6–0.8, and the cross-spectral gain indicates that the amplitude of the reconstruction is a nearly unbiased estimate of the true temperature amplitude. Therefore, this reconstruction should be especially useful for studying multi-decadal temperature variability in the Tasmanian sector of the Southern Hemisphere over the past 3592 years. To this end, we examined the time evolution of low-frequency temperature amplitude fluctuations and found evidence for a 35% amplitude reduction after AD 100 that persisted until about AD 1900. Since that time, the low-frequency temperature amplitude has systematically increased. We also show how this reconstruction is related to large-scale sea surface temperatures (SST) in the Indian Ocean and eastward to the dateline. Pointwise correlations between the Tasmanian record and SSTs reveal a relationship that extends across the southern Indian Ocean and towards the Arabian Sea. This pattern is largely determined by inter-decadal temperature variability, with correlations in this >10-year bandwidth commonly exceeding 0.6 over most of the southern Indian and southwestern Pacific sectors. A rotated empirical orthogonal function analysis reveals that the pattern of pointwise correlations found between the temperature reconstruction and SSTs is largely explained by the linear combination of three orthogonal modes of SST variability.

E. R. Cook (✉) · B. M. Buckley · R. D. D'Arrigo
Lamont-Doherty Earth Observatory, Palisades, NY 10964, USA
E-mail: drdendro@ldeo.columbia.edu

M. J. Peterson
Forestry Tasmania, Hobart, Tasmania, Australia

1 Introduction

This study describes the newest results in a long-term dendrochronological project in Tasmania, Australia aimed at developing and applying multi-millennial tree-ring chronologies to the study of past climatic and environmental change. The emphasis here is on research conducted on Mt. Read in western Tasmania where a recently discovered, disjunct stand of sub-alpine Huon pine (*Lagarostrobos franklinii* C.J. Quinn) has produced a high-quality record of past warm-season (November-April) temperatures covering the past few millennia. Here we describe the extension of the Mt. Read tree-ring chronology back over 4000 years into the past using a method that preserves more low-frequency climate variability in the chronology. In addition, we improve the quality of the temperature estimates derived from the tree-ring series and show how useful these estimates are in the time and frequency domains. In particular, we demonstrate that the amplitude of low-frequency (>10 year) temperature variability in the reconstruction is a nearly unbiased estimate of the true low-frequency temperature amplitude in instrumental data. Finally, the temperature reconstruction is shown to reflect large-scale variability in sea surface temperatures (SST) from the Indian Ocean eastward to the dateline. This large-scale variability is mostly contained in three orthogonal SST modes estimated by rotated empirical orthogonal function analysis (sensu Richman 1986).

The reconstruction of past warm-season surface air temperatures over Tasmania from Huon pine tree rings has undergone a number of developments, analyses, and improvements since its first description by Cook et al. (1991, 1992). In those papers, the authors described the development of a 1089-year tree-ring chronology from

living Huon pine trees growing at an upper-treeline, subalpine location on Mt. Read in western Tasmania. The ring-width variations of this record were shown to reflect patterns of warm-season average temperature over Tasmania, and a well-verified quantitative reconstruction of past temperatures back to AD 900 was produced (Cook et al. 1992). As a result, it was possible to show that the anomalous warming occurring over Tasmania since 1965, as indicated by instrumental temperatures since 1885, was likely to be the warmest such event of the past 1000 years. This finding placed the current warming in a much longer historical perspective, and added new support for the existence of anomalous twentieth century warming over much of the globe.

Spectral analysis of the 1089-year temperature reconstruction indicated the presence of statistically significant ($P < 0.05$) peaks with periods of 30, 56, 80, and 180 years. These "signals" were not investigated further, except to note that they possibly reflected the internal dynamics of the coupled ocean-atmosphere-cryosphere system in the Tasmanian sector of the Southern Ocean.

At about the time of the Cook et al. (1992) report, a large quantity of sub-fossil Huon pine wood was discovered at the site on Mt. Read. This discovery led to the extension of the Huon pine chronology back to 300 BC, which resulted in a new temperature reconstruction that more than doubled the length of the previous record (Cook et al. 1995b). The new 2290-year reconstruction indicated that the post-1960 warming over Tasmania was still highly anomalous, but probably not unprecedented. Spectral analyses of this record verified the presence of the previously identified oscillatory modes over this much longer time interval, with mean periods of 31, 56, 79, and 204 years, suggesting that they truly reflect long-term, natural modes of temperature variability. Consequently, they were investigated for links to possible forcings. In so doing, some statistical (albeit tenuous) evidence was presented for links between the 79 and 204 year modes and solar forcing at Gleissberg and longer time scales.

With the collection and dating of additional sub-fossil Huon pine wood from Mt. Read, Cook et al. (1996a) extended the Tasmanian temperature reconstruction back to 800 BC. New spectral analyses of this 2792-year reconstruction again verified the probable existence of the previously identified inter-decadal and century-scale oscillatory modes, now with mean periods of 31, 56, 78, and 200 years. Using singular spectrum analysis (Vautard et al. 1992), Cook et al. (1996a) showed that these oscillatory modes were present throughout the record, but were strongly amplitude modulated. Collectively, they explained about 12% of the variance in the unfiltered temperature reconstruction and about 41% of variance in the 10-year low-pass filtered reconstruction. Interestingly, these modes could also account for approximately 51% of the warming over Tasmania since 1965, with the remaining 49% due to other processes. Finally, Cook et al. (1996a) showed how these natural oscillatory modes could theoretically mask future warming trends over Tasmania due to greenhouse gas forcing.

Cook et al. (1996b) investigated the possible link between the recent increase in Huon pine ring widths on Mt. Read and natural climate variability, CO_2 fertilization, and greenhouse warming. Several lines of argument were put forth to show that CO_2 fertilization was unlikely to be a contributor to the growth increase. This was accomplished through comparisons of the Huon pine record with independent records of sea surface temperature and atmospheric circulation affecting Tasmania. In so doing, Cook et al. (1996b) showed that the recent growth increase was totally consistent with an increase in warm-season temperatures, a relaxation of the zonal westerlies, and a southward migration of the sub-tropical high pressure belt off the eastern coast of Australia. None of these comparisons could directly test the greenhouse warming hypothesis because of the way it may be entwined in the measures of "natural climate variability" affecting Tasmania.

Finally, Buckley et al. (1997) showed through the analysis of an elevational transect of Huon pine chronologies in Tasmania how the upper elevation Mt. Read site appears to be uniquely suited for the study of warm-season temperatures from its ring widths.

2 A new Mt. Read Huon pine tree-ring chronology

Since the Cook et al. (1996b) study, a great deal of progress has been made in improving the multi-millennial temperature reconstruction from the high-elevation Huon pine site on Mt. Read in western Tasmania. This work has involved the addition of a large set of new tree-ring data from sub-fossil wood collected from the site in February 1997. This new collection has increased the sample size in the pre-1000 BC period considerably and has also extended the useful period of record back to 1600 BC.

Figure 1A shows the mean ring-width series with sample size information below it. The complete time period covered is 2146 BC-AD 1990, which makes this chronology the longest such record in the Southern Hemisphere and one of the longest in the world. The sample size averages around 50 ring-width measurements per

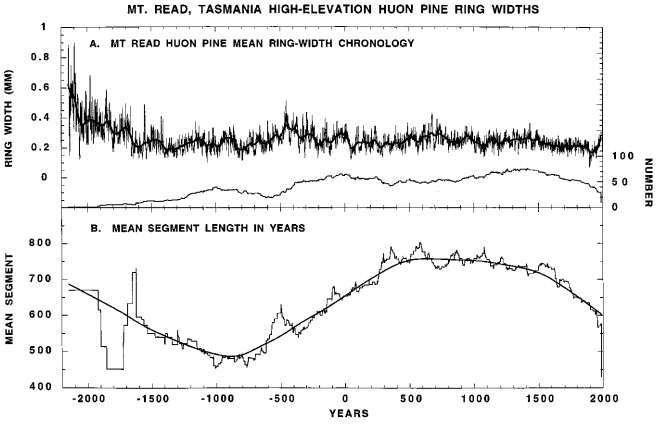

Fig. 1A, B The Mt. Read Huon pine **A** mean raw ring-width data and **B** mean segment lengths, with the number of measurements per year indicated

year back to 600 BC, 25 in the 1200–600 BC period, and 10 in the 1600–1200 BC periods. This is a substantial improvement over the previously published Huon pine record (Cook et al. 1996a), which extended back to 800 BC with only 15 measurements per year on average prior to AD 900.

Figure 1B shows the mean segment lengths for each year. The mean segment lengths are important information for understanding the potential loss of low-frequency climatic variance due to standardizing the individual ring-width series, see Cook et al. (1995a) for details regarding this "segment length curse". In any case, the mean segment lengths range from 500 to 800 years, with the minimum occurring approximately 3000 years ago. If the individual ring-width series were detrended independently of each other, then the maximum resolvable low-frequency variance would be on the order of 500–800 years, probably less in many cases. In an effort to preserve low-frequency climatic variance in excess of the individual segment lengths, we applied the regional curve standardization (RCS) method of Briffa et al. (1992, 1996) to the data.

The substantial increase in sample depth has allowed us to use this much more conservative, albeit noisier, method of RCS tree-ring standardization (Briffa et al. 1992, 1996). The RCS method allows for the preservation of low-frequency variance in excess of the lengths of the individual segments used in creating the full-length tree-ring chronology. Briffa et al. (1992, 1996) and Cook et al. (1995a) showed how all traditional methods of tree-ring standardization limit the preservation of maximum low-frequency variance to the lengths of the individual segments used in constructing the composite mean chronology.

The RCS method requires that the ring-width measurements be aligned by biological age to estimate a single mean growth curve that reflects the intrinsic trend in radial growth as a function of age. The biological age of the rings (i.e., the number of years from the pith) is not known precisely here for most of the tree-ring specimens. However, it appears that the RCS method is not very sensitive to this uncertainty, especially when juvenile growth has relatively little trend (PD Jones, personal communication). Such is the case here. Figure 2A show the mean ring-width series of the individual radial growth series after they have been aligned by biological age. The corridor of points around the mean are the 2-standard error limits of the mean series. Also shown is the sample size as a function of years from pith. The mean series declines in a reasonably systematic and simple way as a function of age. The simplicity of this ring-width decline with increasing age indicates that the RCS method may work well here. The mean value function does become more erratic however as the number of measurements per year declines. Yet even out to the end the slope of the trend remains consistent.

The RCS growth curve data decline with time in a way that is also consistent with the general increase in the average biological age of the trees in the ensemble. This is illustrated in Fig. 2B, where the mean biological age of the wood used in the mean tree-ring chronology is shown. Overall, the trend is positive, indicating the use of increasingly older trees in the mean value function.

The mean series shown in Fig. 2A is not used to standardize the individual tree-ring series because it is clearly noisy. Therefore, a simple theoretical growth curve has been fit to the mean series. This RCS curve is shown in Fig. 2A as the smooth curve superimposed on the mean series. As can be seen, it is almost always within the 2-standard error limits of the mean series. Therefore, it appears to be an adequate estimate of the intrinsic biological age trend of Huon pine growing on Mt. Read over the past 4000 years. This fitted growth curve will be used to detrend and standardize all of the individual ring-width series.

Figure 3A shows the resulting Mt. Read RCS tree-ring chronology. Superimposed on it is a smoothing spline designed to emphasize fluctuations longer than 50 years in duration. The sample size information is the same as that in Fig. 1A. This sample size information has been used to correct the variance of the mean chronology for changing sample size in a theoretically correct way (Osborn et al. 1997). Comparing the mean series in Figs. 1A and 3A, it is clear that the RCS method has removed some long-term growth variations in the standardized chronology, but much of the century-scale information has been preserved. Figure 3B shows a running series of average correlation (RBAR) and expressed population signal (EPS) statistics that illustrate the strength of the common signal in the RCS chronology (Wigley et al. 1986). The RBAR statistic is the average correlation between all possible series in any given 100 year window with 50-year overlap. So, it acts as a running measure of percent common variance, or common signal strength. The error bars are 2-standard error limits. The RBAR runs between 0.2–0.3 over most of the past 4000 years, but shows a conspicuous deterioration in precision before about 1600 BC due to declining sample size. The running EPS statistic is the correlation between the sample chronology developed here and the theoretical population chronology based on an infinite number of samples. The dashed line delineates a EPS threshold of 0.80. So, it is apparent that the RCS chronology has an EPS in excess of 0.80 as far back as 1600 BC, before which it declines due to declining sample size. Based on these measures of signal strength, we determined that the RCS chronology was reliable for further dendroclimatic analysis back only as far as 1600 BC.

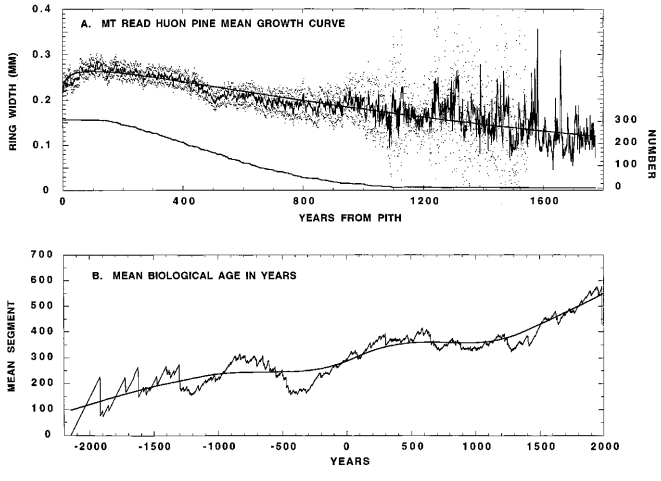

Fig. 2A, B The RCS curve used **A** for standardization and **B** the mean biological age of the wood over time all based on the raw ring-width data shown in Fig. 1A

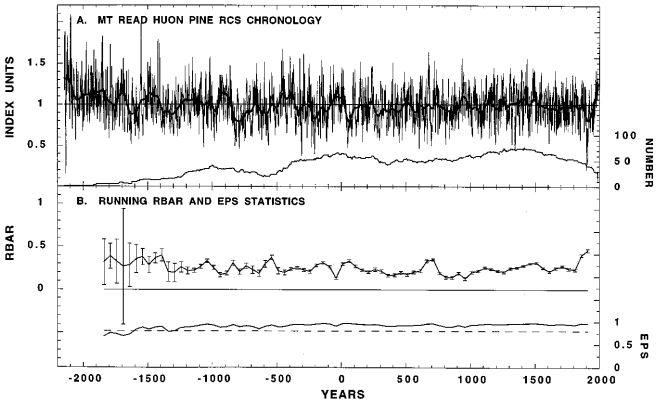

Fig. 3 **A** The Mt. Read RCS tree-ring chronology and **B** its running RBAR and EPS statistics. These statistics are measures of common signal strength amongst the individual series. The moving window used for computing the RBAR and EPS statistics is 100 years with 50 year overlaps. The 2-standard error limits on the RBAR plot indicate that the chronology is probably not reliable prior to 1600 BC

2.1 Robust autoregressive (AR) prefiltering

We have experimented with a robust autoregressive (AR) prefiltering method (Kleiner et al. 1979; Martin and Thomson 1982) to eliminate innovational outliers in the Huon pine chronology prior to its use in reconstructing past warm-season temperatures. This was done because of some clear lack of fit between the tree rings and instrumental temperatures in the 1899–1915 period due to extreme growth suppression in the Huon pine (see Cook et al. 1992). This suppression resulted in the systematic underestimation of actual temperatures.

The innovations being tested as outliers are equivalent to the white noise residuals or random shocks described by Box and Jenkins (1970) for AR processes. These innovations are assumed to be normally distributed $N(0,\sigma)$. So, an innovational outlier is simply an extreme white noise residual resulting from an AR model fitted to the observations. See Fox (1972) for a more detailed discussion of outliers in time series.

Using the method described in Kleiner et al. (1979), innovational outliers were identified in the Huon pine series after AR model fitting and appropriately down-weighted or deleted, depending on their magnitudes. This procedure approximated the classic 3σ hard-rejection rule for the elimination of outliers in statistical samples. The resulting modified innovations were then used in combination with the AR model coefficients to recreate the original series minus the effects of the innovational outlier(s). This process was repeated until no new outliers were identified and removed. In so doing, we objectively identified and eliminated two extreme tree-ring innovations associated with the 1898 and 1908 growth years (see Fig. 3A), two years that had been previously noted as outliers by Cook et al. (1992). Several additional outliers were also identified and removed back to 1600 BC. These are shown in Fig. 4A. The majority are negative and much more severe then those occurring in 1898 and 1908.

We interpret the negative outliers as expressions of unseasonable, short-term outbreaks of cold air over Mt. Read during the growing season. This interpretation is supported by a report from a small mining village that existed near the summit of Mt. Read in 1898–1899. It reported that there was snow on the mountain in January, 1899 (part of the 1898–99 growing season), and the month in general was "more like July than January", i.e., more like winter than summer. Thus, the Huon pines were probably damaged by the unseasonably cold weather, resulting in a non-linear reduction in growth that was inconsistent with the average temperature for the overall growing season. Unfortunately, by 1908 the village on Mt. Read was abandoned. Thus, no equivalent extreme weather report exists for the 1908–1909 growing season. The transient response of the Huon pines to these inferred cold injury events apparently lasted several years (see Fig. 4B) due to the AR-modeled physiological persistence in the tree rings. As a result, radial growth in the 1898–1915 period was anomalously below that allowed for by the average growing season temperatures during that time period.

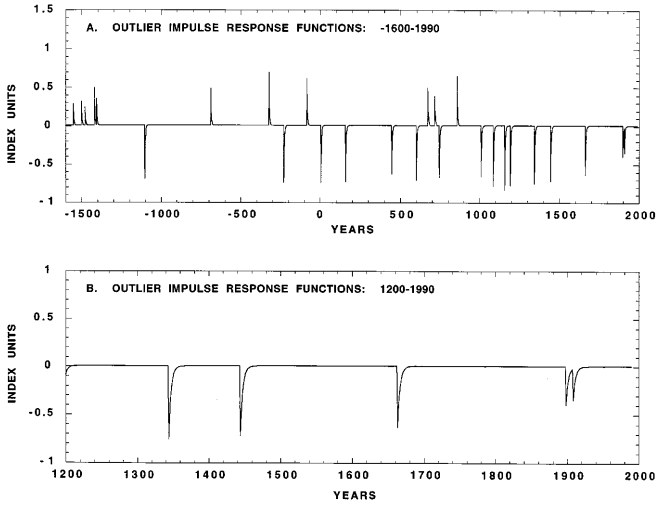

Fig. 4A, B The impulse response functions produced by the outliers removed by robust AR prefiltering. All are shown in **A**, while **B** an expanded view of the AD 1200–1991 period is shown to illustrate the exponential decay of the impulse response functions for clearly

3 A new warm-season temperature reconstruction

We have developed two new warm-season temperature reconstructions from the Mt. Read Huon pine RCS chronology, one based on the original (i.e., unfiltered) series and one based on the robust AR prefiltered series. The effect of AR prefiltering on the calibration and verification statistics is shown in Fig. 5A–C. For the 1920–1991 calibration period, both the original and AR

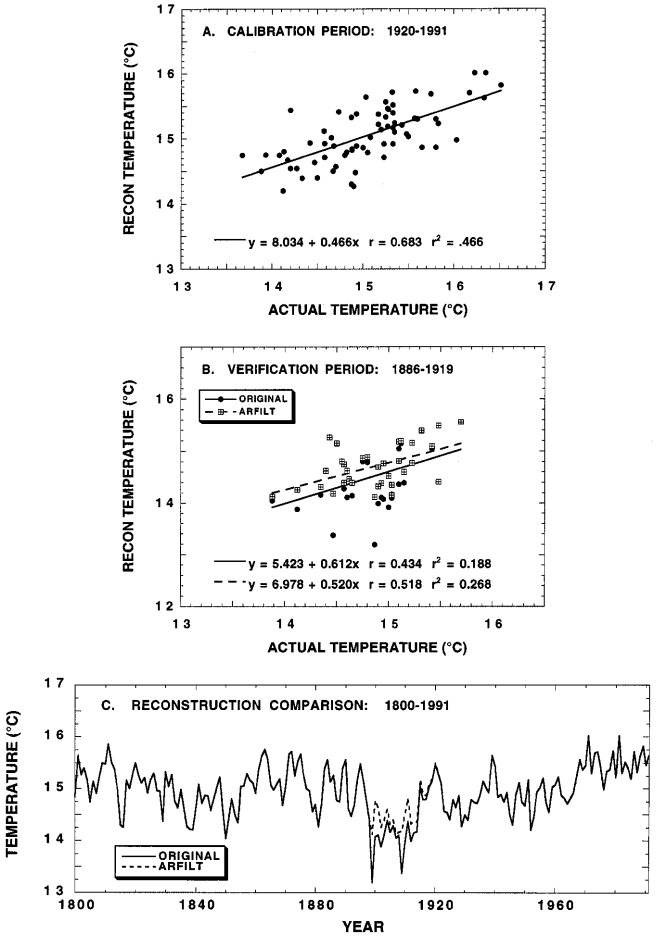

Fig. 5A–C Calibration and verification results using the RCS tree-ring chronology to reconstruct warm-season (November–April) temperatures over Tasmania. This was done using the chronology in its original form and after robust AR prefiltering to remove innovational outliers in the years 1898 and 1908. **A** The 1920–1991 calibration is the same using each chronology because no outliers were found in that period. **B** The 1886–1919 verification results indicate that the reconstruction based on the prefiltered chronology is a better estimate of temperature. **C** The zone of improvement covers the period 1899–1915 where the two innovational outliers were removed

prefiltered chronologies produced identical results because no outliers were identified in that period. The R^2 was 46.6%, an increase over previous models of about 7% (e.g., Cook et al. 1992). In the 1886–1919 verification period, the prefiltered series estimate temperatures better than the original series after the elimination of the outliers. The r^2 (i.e., the square of the Pearson correlation) is 26.8% for the former and 18.1% for the latter. The slope of the line fit to the verification data (Fig. 5B) is also closer to that fit to the calibration data (Fig. 5A) when the prefiltered data are used. Therefore, the temperature reconstruction based on the prefiltered RCS chronology appears to be the best one to use.

Figure 5C shows the original and prefiltered temperature estimates over the 1800–1991 period. The only difference between them occurs locally in the 1899–1915 period where the outliers were removed. Note that the effect of removing innovational outliers extends after their years of occurrence. The duration of this effect on the temperature estimates depends on the operational duration of the impulse response function of the AR process fit to the series. In this case, the AR model was order-1, which means that the impulse response function decays exponentially with time (see Fig. 4). It is arguable that the outliers removed from the RCS chronology represent true climate information. Thus by removing them, some potentially valuable information on extreme events has been lost. We do not necessarily debate this assertion. Indeed, the chronology of extreme events shown in Fig. 4A may prove quite useful for certain lines of interpretation in its own right. However, for our present purposes, we are more interested in the multi-decadal time scale of climate variability, and these outliers may represent more of a liability than an asset in this context.

To see how we affected the spectral properties of the temperature reconstruction by removing the outliers, we performed a cross-spectral analysis on the actual and estimated temperatures over the common period 1886–1991 using the multi-taper method (Thomson 1982) with five 4-pi tapers. This was done for both the unfiltered and prefiltered estimates. These results are shown in Fig. 6. The power spectra plotted on log scale (Fig. 6A) show the distribution of variance as a function of frequency in each series. The spectra of both tree-ring estimates are similar over all frequencies, and each systematically underestimates the power in the actual temperatures at periods shorter then about 12 years. At periods longer then 12 years, the spectral power in the actual and estimated temperatures is very similar. The coherency spectra in Fig. 6b provide estimates of relative agreement between the actual and estimated temperatures as a function of frequency and can be interpreted as a series of squared Pearson correlation coefficients (i.e., r^2) in this context. They reveal clearer differences between the two tree-ring estimates. In general, the prefiltered reconstruction is more coherent then the unfiltered one even though each was based on the identical calibration equation. So, this difference must be due to the elimination of the two innovational outliers.

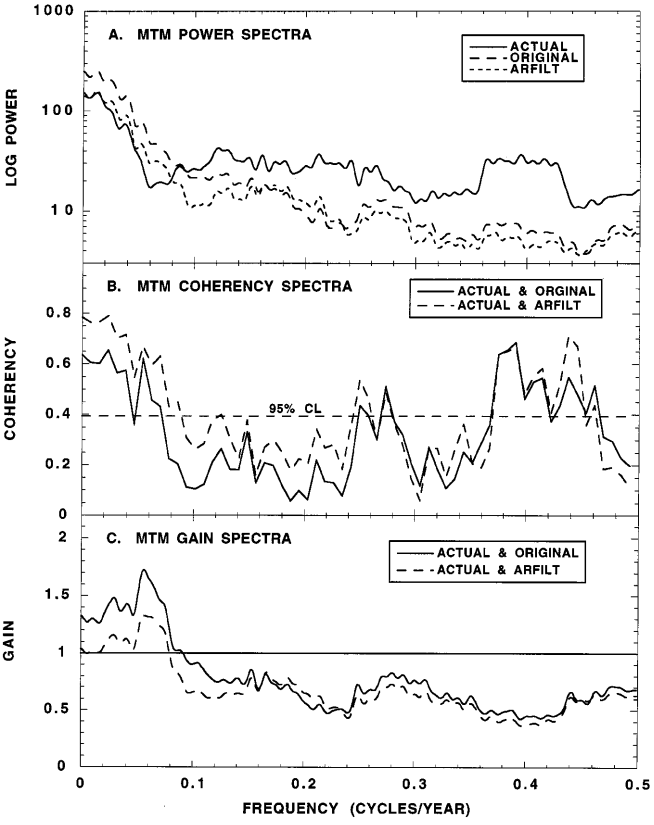

Fig. 6A–C Cross-spectral analyses of the unfiltered and prefiltered temperature estimates with the actual data over the period 1886–1991. The reconstructions do a better job at reconstructing the actual temperature amplitude at periods >12 years in length then at shorter periods (see **A**, **C**), with the robust AR prefiltered series being nearly unbiased at inter-decadal timescales. **B** The coherency spectra indicate that the prefiltered reconstruction is better related to the actual data at periods longer then 4 years then is the unfiltered reconstruction

The improved coherence in the prefiltered estimates is especially evident at periods longer then 4 years. This is understandable given the effect of outlier removal on the estimates shown in Fig. 5C. At periods longer then 12 years, the coherency of the prefiltered estimates exceeds 0.6, which is a substantial improvement over the unfiltered estimates. The gain spectrum (Fig. 6C) describes the passage of temperature amplitude as a function of frequency in a linear input-output model sense, with the regression model acting as the filter. It shows in a different way the same basic results as the power spectra. That is, the greatest loss of amplitude is at periods shorter then 12 years. Over the 12–2 year bandwidth, the amplitude of the output signal is typically 0.3–0.4 that of the input signal. However, at periods longer then 12 years, the temperature amplitude passed is >0.75 that of the input signal. The main difference between the unfiltered and prefiltered series is an indication of inflated amplitude in the former at a period of about 25 years. So, the amplitude of temperature variability in the AR prefiltered reconstruction appears to be an accurate, nearly unbiased, estimate of the true temperature amplitude at periods >12 years.

Overall, the cross-spectral analyses with the instrumental data indicate that the reconstruction based on the AR prefiltered tree-ring chronology is better than the unfiltered one. The prefiltered estimates are generally more coherent with the actual temperatures, especially at periods longer then 12 years. However, both of the reconstructions is biased in the same systematic way. That is, they both significantly underestimate the true amplitude of temperature variability at periods shorter then 12 years. At periods longer then 12 years they more accurately reflect the true amplitude of variability found in the actual temperatures. Between this result and the very high coherency in the same low-frequency bandwidth, it is clear that the Tasmania warm-season temperature reconstruction is most reliable for providing estimates of natural variability on decadal to centennial time scales. At shorter wavelengths, the coherency of the estimates is still reasonably good, but more care must be taken in deriving estimates of high-frequency natural variability from the reconstruction.

We applied one final test to the unfiltered and AR prefiltered reconstructions to see if any longer-term systematic bias due to outlier suppression might be evident in the latter series. This was done because most of the outliers removed from the tree-ring chronology came from the pre-instrumental time period. We computed the power spectra of the original and prefiltered reconstructions along with their coherency spectrum. These spectra (not shown) indicated virtually no significant difference between the two reconstructions. Indeed, the coherency spectrum revealed that the two series have $>85\%$ variance in common over most frequencies. Since there is no clear evidence for systematic bias in the AR prefiltered reconstruction, its use in further analyses of multi-decadal temperature variability is justified.

The new warm-season temperature reconstruction and its 50-year low-pass filtered version, based on the RCS method of tree-ring standardization and AR prefiltering, is shown in Fig. 7. It covers the period 1600 BC-AD 1991. Concentrating on the low-pass series for now, it is apparent that the current warming trend over Tasmania is still a significant event when viewed in the context of multi-decadal variability covering the past 2000 years. In that period it remains the warmest event to a marginal degree, although a much longer warm period is indicated in the AD 900–1500 interval. The early 1900s period likewise remains a significant cold event, although it was apparently exceeded several times over the past 2000 years, with the coldest event occurring around AD 50. There is little indication for a "Little Ice Age" period of unusual cold in the post-1500 period. Rather, the AD 1500–1900 period is mainly characterized by reduced multi-decadal variability.

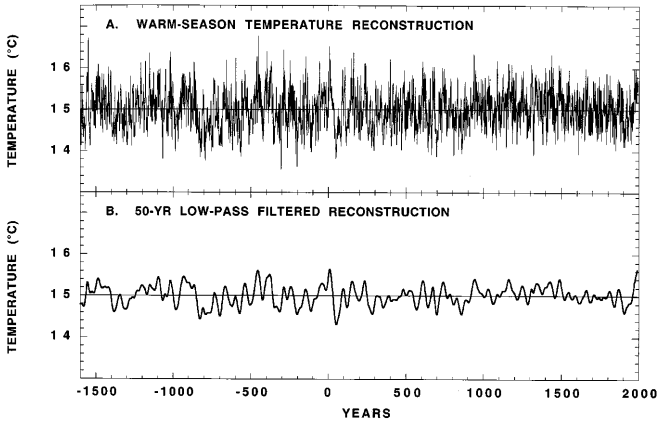

Fig. 7 **A** The prefiltered warm-season Tasmania temperature reconstruction and **B** the same series in 50-year low-pass filtered form, covering the period 1600 BC-AD 1991

The properties of the reconstruction over the past 2000 years are highly consistent with those published previously (Cook et al. 1991, 1992, 1995b, 1996a), although there does appear to be a stronger indication in the present record for persistent warmth in the AD 900–1500 period. What clearly stands out in the new reconstruction is the pattern of much greater variability prior to AD 100. This increase in variability is visibly apparent in both the unfiltered and low-pass filtered series. As a consequence, between 1600 BC and AD 100, we have the most extreme single-year and multi-year warm and cold events of the past 3592 years. Given the substantial tree-ring sample depth for most years in this series and the fact that the series had its variance adjusted to take into account the effect of changing sample size, there is little reason to suspect that this change in variance is a data artifact.

In order to take a close look at this change in variability, we transformed the reconstruction in Fig. 7A into absolute departures from the mean and low-pass filtered them with a 200-year smoothing spline. This produced a time series of local temperature amplitude variations. The same procedure was also applied to the absolute departures of the 50-year low-pass filtered reconstruction (Fig. 7B) and its 50-year high-pass counterpart. As described earlier, the amplitude of the 12-2 year bandwidth is significantly underestimated, so more care must be exercised in interpreting changes in this series. The temperature amplitude series (Fig. 8A–C) again show that the amplitude of temperature variation was generally higher before AD 100. This is especially evident in the amplitude series of the 50-year low-pass series (Fig. 8B) and much less so in the high-pass series (Fig. 8C). This indicates that the change in amplitude was mainly driven by low-frequency, multi-decadal variations in the temperature reconstruction. Indeed, Fig. 8B suggests that an abrupt reduction in the amplitude of low-frequency temperature variability occurred approximately 1900 years ago as highlighted by the mean amplitude lines drawn in. This reduction, from 0.225 °C to 0.147 °C, was largely sustained until the 1800s. Since 1900, the trend in amplitude appears to be increasingly dominated by low-frequency patterns of change, which suggests a return to more persistent temperature anomalies seen some 2000 years earlier. Thus, the current warming trend over Tasmania, which

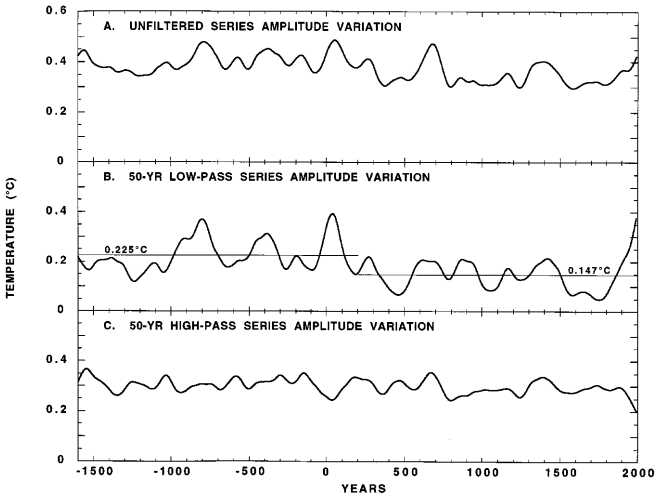

Fig. 8A–C Plots of local temperature amplitude changes based on smoothing the absolute values of the temperature departures with a 200-year smoothing spline. This was done on **A** the yearly reconstruction, **B** its 50-year low-pass component, and **C** its 50-year high-pass counterpart. These plots highlight the increase in variability prior to AD 100 and show that most of that increased variability is due to low-frequency amplitude changes in the series

began in the 1960s, may in part be a manifestation of this return to the more persistent anomalies of the past that dominated Tasmanian warm-season temperatures (see Cook et al. 1996a).

4 Spectral analysis

Cook et al. (1995b, 1996a) described the spectral properties of earlier versions of the long Tasmania temperature reconstruction. In so doing, they documented the probable occurrence of stable, long-term, multi-decadal and century-scale oscillations in the series with mean periods of approximately 31, 57, 78, and 200 years. These oscillations were found to exist in the series as far back as 800 BC (Cook et al. 1996a). Cook et al. (1996a) also illustrated how the combination of these four oscillations alone could explain approximately half of the warming that has occurred over Tasmania since 1960. Here we will examine the spectral properties of our new reconstruction to see how it compares to the earlier ones. We expect that the RCS method of standardization will provide more insights into the low-frequency characteristics of temperature variation through the better preservation of low-frequency variance in excess of that allowed for by the individual segment lengths used in the tree-ring chronology (Cook et al. 1995a).

For this purpose, we have used the multi-taper method (MTM) of spectral analysis (Thomson 1982), with robust estimation of the red noise background spectrum (Mann and Lees 1996). MTM provides very high-resolution spectral estimates and the best possible protection against leakage, while the robust background spectrum provides a better way to determine the statistical significance of band-limited signals embedded in red noise. The MTM spectrum based on three 2-pi tapers is shown in Fig. 9. The full log spectrum over the 0–0.5 frequency range (Fig. 9A) clearly illustrates the red noise character of the process. Several harmonics project above the 95% and 99% confidence levels.

Figure 9B shows an expanded view of the spectrum, plotted on linear scale for the 0–0.05 bandwidth only. All peaks that exceed their associated 95% and 99% confidence levels are indicated. With regards to how these results compare to those of Cook et al. (1995b, 1996a), we find significant power in the 210–260, 68–80, and 31 year bands here. These peaks compare favorably to the 200, 78, and 31 year oscillations described previously. The 57 year band is conspicuously missing however, and the 31 year band is weaker then before. These differences suggest that there has been some drift in the periods of these oscillations over time, a result that should not be surprising given the probable lack of periodic forcing. Indeed, the appearance of such organized band-limited behavior in the reconstruction covering the past 3592 years is rather remarkable. Interestingly, we now have a significant peak at 588 years. This peak was suggested in the spectrum produced by Cook et al. (1996a), but in that case did not exceed the 95% confidence level. The significance ($P < 0.01$) of the 588 year peak found here can be attributed to the RCS method and an increase of 800 years in the series length over that used by Cook et al. (1996a). Thus, band-limited temperature variability at multi-decadal and century scale wavelengths appears to be a persistent feature of the

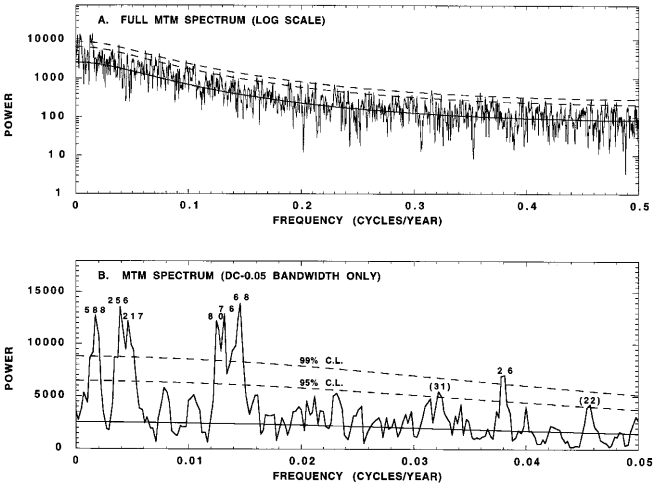

Fig. 9A, B The MTM spectrum of the prefiltered temperature reconstruction with a robust red noise null spectrum fit to it. The 95% and 99% confidence levels are indicated by the *dashed curves*. **A** The full spectrum is shown and **B** shows expanded view of the spectrum over the DC-0.05 bandwidth. The latter clearly shows that the new reconstruction has significant band-limited, multi-decadal and century-scale power, mainly with periods of 210–260 and 68–80 years. In addition, the RCS method has preserved significantly more low-frequency variance such that a 588-year peak of low-frequency variability is now evident

climate system in the Tasmanian sector of the Southern Hemisphere.

It is unlikely that this organized, low-frequency behavior is driven by the internal dynamics of atmospheric circulation alone. Rather, its origin is more likely to come from coupled ocean-atmosphere dynamics and, perhaps, from changing solar irradiance that affects the heat content of the upper ocean layer (White et al. 1997). For example, spectral analysis of annual average surface air temperatures for the Southern Hemisphere produced by a 1000 year control run of a coupled ocean-atmosphere model (Delworth et al. 1993) indicated the presence of unforced band-limited power at multi-decadal and century time scales (Cook et al. 1995b). We have also examined warm-season SSTs, averaged over the southern Indian Ocean, that were generated by a 1400 year control run of the Hadley Centre coupled ocean-atmosphere model (HADCM2; Johns et al. 1997; Tett et al. 1997). This record (detrended for a small amount of model drift) and its multi-taper power spectrum are shown in Fig. 10. At interdecadal and century time scales, the model-generated SSTs have band-limited spectral features that are remarkably similar to the Huon pine reconstruction, all without any changes in external forcing (e.g., solar). Assuming that the temperature reconstruction accurately reflects true low-frequency SST variability in the southern Indian Ocean, our record supports the usefulness of the HADCM2 model for generating realistic unforced low-frequency warm-season SST variability in this sector. In turn, the HADCM2 results suggest that natural processes, such as variations in the Antarctic Circumpolar Current and

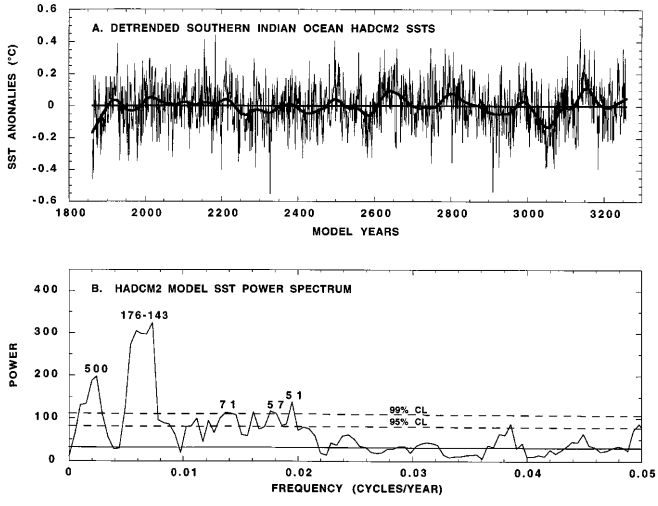

Fig. 10A, B Hadley Centre coupled ocean-atmosphere model (HADCM2) SSTs generated by **A** a 1399-year control run and **B** their multi-taper power spectrum only shown over the DC-0.05 band. The SSTs are warm-season (November–April) averages for the southern Indian Ocean (20–50°S and 25–180°W). They have been detrended for a small amount of model drift and are expressed in anomaly form. Note the clear presence of multi-decadal and century time scale variability that is remarkably similar to the spectrum of the Huon pine temperature reconstruction (Fig. 9)

Fig. 11A–C Indian Ocean warm-season SST correlations with the Tasmanian temperature reconstruction. The correlations are shown for **A** unfiltered, **B** 10-year high-pass, and **C** 10-year low-pass data. Statistically significant correlations are indicated over most of the Indian Ocean south of 30° all the way west to southern Africa, with most of the large-scale correlation structure in the low-pass band. This result indicates that the reconstruction is reflecting large-scale patterns of climatic variability and change in the Southern Hemisphere

remote forcing by Indonesian throughflow (Allan et al. 1995; Reason et al. 1996), may be driving the low-frequency band-limited behavior in the temperature reconstruction.

This being said, Cook et al. (1995b) did examine an earlier Tasmania temperature reconstruction for possible links to solar forcing at periods of ~80 years (the Gleissberg sunspot cycle) and ~200 years (as indicated in high-precision radiocarbon measurements; e.g., Sonnet 1984). While not conclusive, these comparisons indicated some reasonably strong evidence for long-term solar forcing in the temperature reconstruction at these time scales. Our present record remains consistent with those findings. We also note an interesting correspondence between unusual cold periods in the reconstruction around 800 and 300 BC (see Fig. 7B) and very pronounced "wiggles" in the residual tree-ring $\Delta^{14}C$ record (Damon et al. 1989; Stuiver and Braziunas 1993), which are comparable in magnitude to the unusually strong $\Delta^{14}C$ wiggles during the Maunder and Spörer minima (Eddy 1976). Unfortunately, our reconstruction does not show any evidence for unusual cold during those latter epochs (see Fig. 11 in Cook et al. 1995b). Finally, we note that the significant 588-year spectral peak in our new record is reasonably close to spectral peaks found in residual tree-ring $\Delta^{14}C$ records analyzed by Sonnet (1984) and Stuiver and Braziunas (1993), especially over the $\Delta^{14}C$ time interval comparable to our reconstruction. Stuiver and Braziunas (1993) argue that the ~500-year term in the $\Delta^{14}C$ record is an "ocean mode $\Delta^{14}C$" oscillation that reflects changes in North Atlantic deep water formation and ocean ventilation. If true, then the 588-year spectral peak in the reconstruction is most likely an internally driven phenomenon not directly linked to solar variability and forcing, thus making it consistent with the HADCM2 SST power spectrum results. In contrast, Stuiver and Braziunas (1993) argue that the ~80 and ~200 year terms more likely reflect a direct solar forcing effect on atmospheric ^{14}C production ("solar mode $\Delta^{14}C$"). So, our extended reconstruction may yet support the solar forcing hypothesis as well.

5 Links to large-scale SST anomalies

The warm-season temperature reconstruction from Tasmania covering the past 3592 years is a significant development in Southern Hemisphere paleoclimatology. However, it would be even more useful if it could be

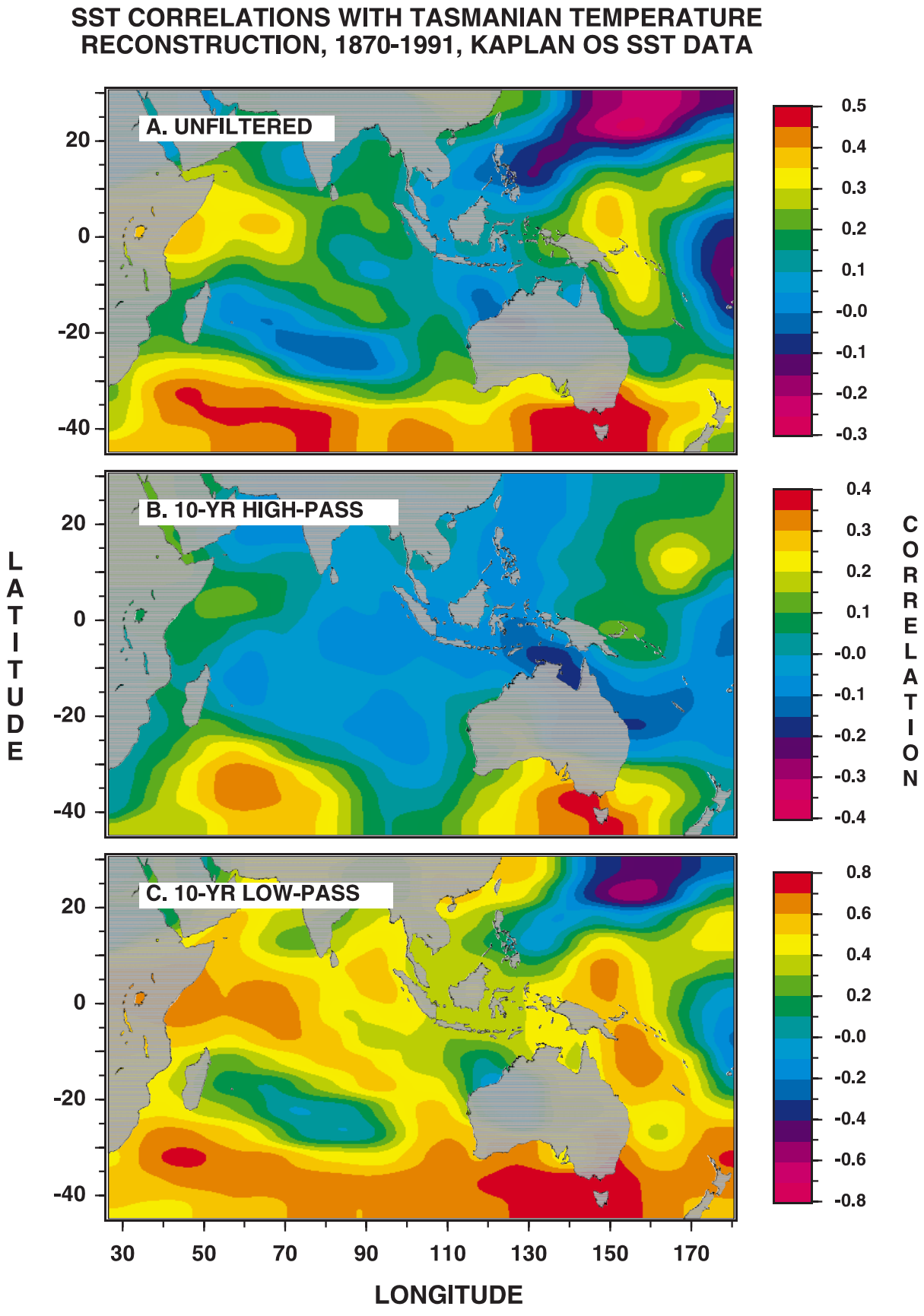
SST CORRELATIONS WITH TASMANIAN TEMPERATURE RECONSTRUCTION, 1870-1991, KAPLAN OS SST DATA
A. UNFILTERED
B. 10-YR HIGH-PASS
C. 10-YR LOW-PASS
LATITUDE
20
0
-20
-40
LONGITUDE
30
50
70
90
110
130
150
170
CORRELATION
0.5
0.4
0.3
0.2
0.1
-0.0
-0.1
-0.2
-0.3
0.4
0.3
0.2
0.1
-0.0
-0.1
-0.2
-0.3
-0.4
0.8
0.6
0.4
0.2
-0.0
-0.2
-0.4
-0.6
-0.8

shown that it relates to larger-scale patterns of climate variation than just those over Tasmania. Cook et al. (1996b) compared an earlier version of the Tasmania temperature reconstruction with sea level pressure records, derived zonal circulation indices, an index of the latitude of the subtropical high pressure belt off eastern Australia, and sea surface temperatures (SSTs) around Tasmania. They showed that most of the inter-decadal warm-season temperature variations that have occurred over Tasmania since the late nineteenth century could be explained by changes in atmospheric circulation and SSTs. Here, we expand this analysis to include SSTs over the entire Indian Ocean and eastward to the dateline. The SSTs used for this purpose are from Kaplan et al. (1998) and the comparison period is 1870–1991.

Figure 11A–C shows color contoured maps of correlations of warm-season SSTs with the temperature reconstruction. These maps were produced using 399 $5° \times 5°$ SST grid boxes, with Tasmania located beneath the Australian continent. In Fig. 11A, the correlations are based on the unfiltered annual values of temperature. The colored contours for correlations >0.3 are significant above the 95% confidence level after correcting degrees of freedom for autocorrelation in the series. This map clearly shows that the temperature reconstruction contains considerable information about climate variability extending over much of the southern Indian Ocean to Africa. This relationship extends northward as well towards the Arabian Sea. The highest correlations are, as expected, closest to Tasmania. However, substantial regions have correlations >0.4, and a large area off the coast of southern Africa is correlated above 0.5. Figure 11B–C shows correlation maps for the same temperature data after 10-year high-pass and low-pass filtering. They reveal that the majority of the large-scale correlations between the Tasmanian reconstruction and southern Indian Ocean SSTs are in the inter-decadal band. A similar large-scale teleconnection between glacial advance in New Zealand and drought in South Africa has also been identified by Tyson et al. (1997) in this same sector of the Southern Hemisphere. This teleconnection has been linked to changes in atmospheric circulation, especially that associated with standing wave 3 and the preferred location of its ridges and troughs. This finding indicates that changes in atmospheric circulation may also be contributing to the large-scale signal in the Tasmanian temperature reconstruction.

As another test of the association between Tasmanian temperatures and large-scale SSTs, we performed a rotated empirical orthogonal function (EOF) analysis (sensu Richman 1986) on the field of warm-season SSTs. The orthogonal varimax method was used to rotate the retained unrotated EOFs. This SST field is seriously underdetermined for EOF analysis because there are only 121 observations for each of the 399 grid boxes. To determine the number of EOFs to retain and rotate, we used the Monte Carlo "Rule-N" method of Preisendorfer et al. (1981). For this purpose, we generated 100 random sets of red noise processes, each of order 121×399, with the red noise terms estimated from the SSTs themselves. The random sets were than subjected to unrotated EOF analysis, with the resulting red noise eigenvalue traces used to generate 95% confidence limits for the true eigenvalue trace. In so doing, we found that the first 12 unrotated EOFs of SST were statistically significant, collectively explaining 80% of the total SST variance. These 12 EOFs were than rotated using the orthogonal varimax method.

To determine which varimax factors were most probably related to the Tasmanian temperatures, we performed a two stage correlation analysis. First, we correlated the field of correlations seen in Fig. 11A with each field of varimax factor loadings. The statistical significance of the resulting simple correlations between each pair of fields is difficult to assess because the number of spatial degrees of freedom is much less than the number of grid boxes. For this reason, we also computed the simple correlations between the Tasmanian temperature reconstruction itself and each series of varimax factor scores. We selected a varimax factor if both its loading pattern and its scores were jointly correlated with Tasmanian temperatures above their nominal 99% significance levels. This process resulted in the identification of three SST varimax factors: factors 4, 5, and 10 which collectively accounted for 16.2% of the variance in the SST field.

Figure 12A–C shows these three SST varimax factor maps. Each factor map is labeled with the percent variance it accounts for and its correlation with the field of correlations shown in Fig. 11A. A visual comparison of each factor map with the correlation map clearly indicates where the significant correlations are coming from. In particular, the pattern of loadings in factor number 5 strongly resembles the pattern of significant correlations at two nodes in the southern Indian Ocean near Tasmania and Africa, resulting in a correlation between them of 0.74. Factor number 4, which loads heavily on the SST field around the Philippine Sea, helps explain the origin of the negative correlations in that region in Fig. 11A. This is a more problematic relationship to physically interpret. However, it could reflect some form of remote forcing on southern Indian Ocean circulation, like that by Indonesian throughflow variations on the southern gyre (Allan et al. 1995; Reason et al. 1996). And, factor number 10 explains the node of significant correlation found in the Southern Ocean at about 110°E longitude. This node lies in between the nodes found in factor number 5, as if in quadrature with the factor number 5 pattern. So, even relatively small

Fig. 12A–C The three SST varimax factor patterns most highly correlated with the pattern of correlations seen in Fig. 10A. The percent variance accounted for by each factor pattern and its correlation with the Fig. 10A map are indicated. Each factor map highlights the region(s) with loadings above 0.5. Visual comparisons of these maps with Fig. 10A clearly shows where the overall pattern of correlation between Tasmanian temperatures and SSTs is coming from

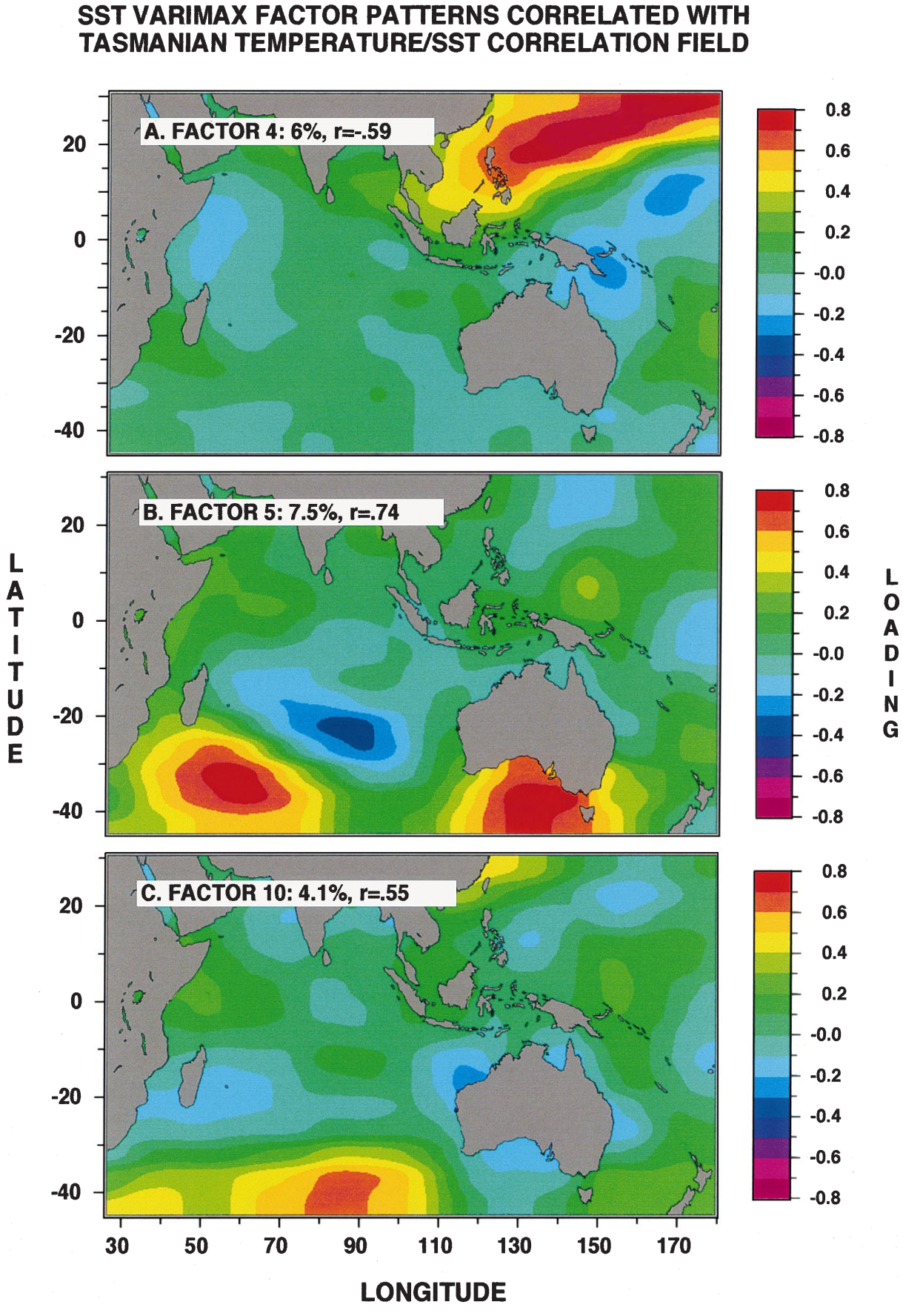
SST VARIMAX FACTOR PATTERNS CORRELATED WITH
TASMANIAN TEMPERATURE/SST CORRELATION FIELD
A. FACTOR 4: 6%, r=-.59
B. FACTOR 5: 7.5%, r=.74
C. FACTOR 10: 4.1%, r=.55
LATITUDE
20
0
-20
-40
LONGITUDE
30
50
70
90
110
130
150
170
LOADING
0.8
0.6
0.4
0.2
-0.0
-0.2
-0.4
-0.6
-0.8

details in the map of correlations are explicable in terms of these three orthogonal modes of SST variability.

To illustrate these relationships further, we show the SST varimax factor scores in Fig. 13A–C. Not surprisingly, the factor 5 scores are most highly correlated ($r = 0.49$) with Tasmanian temperatures. In contrast, the scores of factors 4 and 10 correlate much more weakly ($r = -0.23$ and 0.29, respectively). We have also generated a regression-weighted sum of the factor scores as a best estimate of Tasmanian temperatures (Fig. 13D). The resulting correlation is 0.62, with an equivalent R^2 of 0.384. The percent variance explained by these three SST factors (38.4%) is reasonably comparable to that calibrated by local surface air temperatures over Tasmania (46.6%). Therefore, the pattern of pointwise correlations found between the temperature reconstruction and SSTs can be largely explained by this linear combination of three orthogonal modes of SST variability. In turn, warm-season surface air temperatures over Tasmania are clearly related to large-scale SST anomalies, particularly those in the southern Indian Ocean, with three discrete SST modes being jointly responsible for this relationship.

6 Conclusions

The new warm-season temperature reconstruction is an improvement over previous versions in terms of sample depth, length, and statistical fidelity at inter-decadal and century-scale wavelengths. Spectral analysis of the reconstruction indicates that it is dominated by band-limited, oscillatory patterns of variability with periods of 588, 210–260, 68–80, and 31 years. These results are reasonably consistent with previous results. Similar spectral peaks were also found in southern Indian Ocean SSTs from a 1399 year control run of the HADCM2 coupled ocean-atmosphere model. Assuming that the low-frequency tree-ring oscillations truly reflect past SST variability, then the HADCM2 model appears to be doing an excellent job of producing realistic low-frequency SST variability in the southern Indian Ocean sector. In return, the HADCM2 spectral analysis results suggest that at least some of the low-frequency oscillations observed in the reconstruction are most likely due to internal forcing alone.

The significant correlations found between Indian Ocean SSTs and the land-based reconstructed temperatures are strong evidence for a large-scale climate signal in the Tasmanian record. Indeed, this signal can be largely expressed as the linear combination of three orthogonal modes of SST variability, which in combination influence the passage of cyclones and anticyclones over Tasmania, the temperature of these migratory air masses, and the direction of the prevailing winds.

Somewhat provocatively, the long reconstruction also indicates that the ocean/atmosphere dynamics responsible for inter-decadal and century-scale temperature variability over Tasmania have apparently varied considerably over the past four millennia and were much more variable in the BC time period. This finding suggests that an ocean-mediated climate change occurred about 1900 years ago, which resulted in a generally less variable warm-season temperature regime over Tasmania. Since about 1900, Tasmanian temperatures have become more variable, after about 400 years of remarkably low inter-decadal variability. Thus, Tasmania may now be in a more vigorous phase of climate variability, but one that is still less that seen in the BC time period.

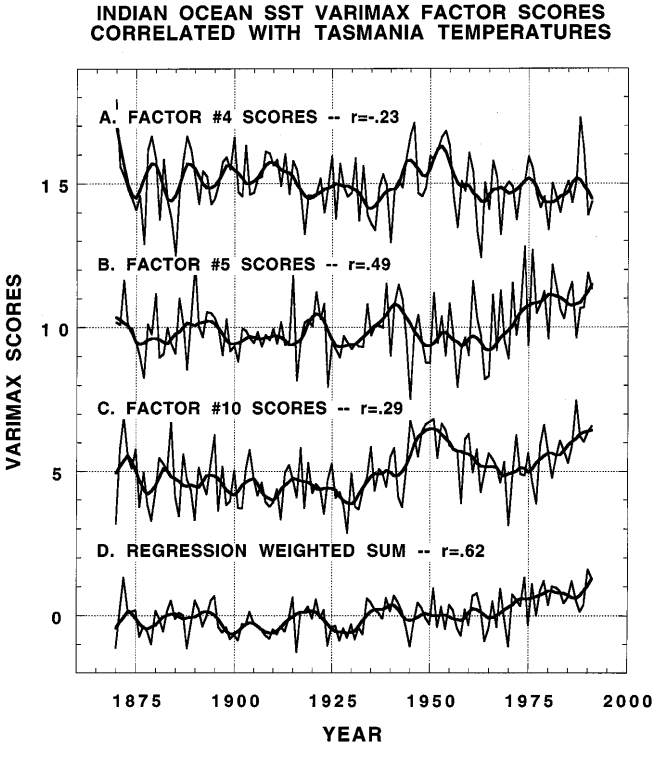

Fig. 13A–D The SST varimax factor scores well correlated ($P < 0.01$) with the **A–C** Tasmanian temperature reconstruction and **D** the regression-weighted sum of those scores. The correlations between these series and the reconstruction are indicated

Acknowledgements We thank T. Bird, R. Francey, M. Barbetti, and K. Allen for field assistance and stimulating discussions, Tim Osborn for providing the HADCM2 southern Indian Ocean SST data through the UK DETR Link project, and M. Mann for providing the MTM spectral analysis programs used here. We also thank the Tasmania Parks and Wildlife Service for long-term permission to conduct dendrochronological research on Mt. Read. Finally, critiques by two anonymous reviewers improved the work and are gratefully acknowledged. This research was supported by the National Science Foundation (Grants ATM 96-27318 and ATM 96-16975). Lamont-Doherty Earth Observatory Contribution No. 5991.

References

Allan RJ, Lindsey JA, Reason CJC (1995) Multidecadal variability in the climate system over the Indian Ocean region during the Austral summer. J Clim 8:1853–1873

Box GEP, Jenkins GM (1970) Time series analysis: forecasting and control. Holden-Day, San Francisco, 553 pp
Briffa KR, Jones PD, Bartholin TS, Eckstein D, Schweingruber FH, Karlen W, Zetterberg P, Eronen M (1992) Fennoscandian summers from AD 500: temperature changes on short and long time scales. Clim Dyn 7:111–119
Briffa KR, Jones PD, Bartholin TS, Schweingruber FH, Karlen W, Shiyatov SG (1996) Tree-ring variables as proxy-climate indicators: problems with low-frequency signals. In: Jones PD, Bradley RS, Jouzel J (eds) Climate variations and forcing mechanisms of the last 2,000 years. NATO ASI Series, vol I41, Springer, Berlin, Heidelberg New York pp 9–41
Buckley BM, Cook ER, Peterson MJ, Barbetti M (1997) A changing temperature response with elevation for *Lagarostobos franklinii* in Tasmania, Australia. Clim Change 36(3–4):245–266
Cook ER, Bird T, Peterson M, Barbetti M, Buckley B, D'Arrigo R, Francey R, Tans P (1991) Climatic change in Tasmania inferred from a 1089-year tree-ring chronology of subalpine huon pine. Science 253:1266–1268
Cook ER, Bird T, Peterson M, Barbetti M, Buckley B, D'Arrigo R, Francey R (1992) Climatic change over the last millennium in Tasmania reconstructed from tree rings. The Holocene 2(3):205–217
Cook ER, Briffa KR, Meko DM, Graybill DA, Funkhouser G (1995a) The segment length curse in long tree-ring chronology development for paleoclimatic studies. The Holocene 5(2):229–237
Cook ER, Buckley BM, D'Arrigo RD (1995b) Decadal-scale oscillatory modes in a millennia-long temperature reconstruction from Tasmania. In: Martinson DG, Bryan K, Ghil M, Hall MM, Karl TR, Sarachik ES, Sorooshian S, Talley LD (eds) Natural climate variability on decade-to-century time scales. National Academy Press, Washington, D.C. pp 523–531
Cook ER, Buckley BM, D'Arrigo RD (1996a) Inter-decadal climate variability in the Southern Hemisphere: evidence from Tasmanian tree rings over the past three millennia. In: Jones PD, Bradley RS, Jouzel J (eds) Climate variations and forcing mechanisms of the last 2,000 years. NATO ASI Series, vol I41, Springer, Berlin, Heidelberg, New York pp 141–160
Cook ER, Francey RJ, Buckley BM, D'Arrigo RD (1996b) Recent increases in Tasmanian Huon pine ring widths from a subalpine stand: natural climate variability, CO_2 fertilization, or greenhouse warming? Pap Proc R Soc Tasmania 130(2):65–72
Damon PE, Cheng S, Linick TW (1989) Fine and hyperfine structure in the spectrum of secular variations of atmospheric ^{14}C. Radiocarbon 31(3):704–718
Delworth T, Manabe S, Stouffer RJ (1993) Interdecadal variations of the thermohaline circulation in a coupled ocean-atmosphere model. J Clim 6:1993–2011
Eddy JA (1976) The Maunder minimum. Science 192:1189–1202
Fox AJ (1972) Outliers in time series. J R Statist Soc, Ser B 43:350–363
Johns TC, Carnell RE, Crossley JF, Gregory JM, Mitchell JFB, Senior CA, Tett SFB, Wood RA (1997) The second Hadley Centre coupled ocean-atmosphere GCM: model description, spinup and validation. Clim Dyn 13:103–134
Kaplan A, Cane MA, Kushnir Y, Clement AC, Blumenthal MB, Rajagopalan B (1998) Analyses of global sea surface temperature 1856–1991. J Geophys Res 103(C9):18 567–18 589
Kleiner B, Martin RD, Thomson DJ (1979) Robust estimation of power spectra. J R Statist Soc, Ser B 41:313–351
Mann ME, Lees J (1996) Robust estimation of background noise and signal detection in climatic time series. Clim Change 33:409–445
Martin RD, Thomson DJ (1982) Robust-resistant spectrum estimation. Proc IEEE 70:1097–1115
Osborn TJ, Briffa KR, Jones PD (1997) Adjusting variance for sample-size in tree-ring chronologies and other regional-mean time series. Dendrochronologia 15:89–99
Preisendorfer RW, Zwiers FW, Barnett TP (1981) Foundations of principal components selection rules. SIO Ref Ser 81-4, Scripps Institution of Oceanography, La Jolla, Ca, USA
Reason CJC, Allan RJ, Lindsey JA (1996) Evidence for the influence of remote forcing on interdecadal variability in the southern Indian Ocean. J Geophy Res 101:11 867–11 882
Richman MB (1986) Rotation of principal components. J Clim 6:293–335
Sonnet CP (1984) Very long solar periods and the radiocarbon record. Rev Geophys Space Phys 22:239–254
Stuiver M, Braziunas TF (1993) Sun, ocean, climate and atmospheric $^{14}CO_2$: an evaluation of causal and spectral relationships. The Holocene 3(4):289–305
Tett SFB, Johns TC, Mitchell JFB (1997) Global and regional variability in a coupled AOGCM. Clim Dyn 13:303–323
Thomson DJ (1982) Spectrum estimation and harmonic analysis. Proc IEEE 70:1055-1096
Tyson PD, Sturman AP, Fitzharris BB, Mason SJ, Owens IF (1997) Circulation changes and teleconnections between glacial advances and the west coast of New Zealand and extended spells of drought years in South Africa. Int J Clim 17:1499–1512
Vautard R, Yiou P, Ghil M (1992) Singular spectrum analysis: a toolkit for short noisy chaotic time series. Physica D 58:95–126
White WB, Lean J, Cayan DR, Dettinger, MD (1997) Response of global upper ocean temperature to changing solar irradiance. J Geophys Res 102(C2):3255–3266
Wigley TML, Briffa KR, Jones PD (1986) On the average value of correlated time series, with applications in dendroclimatology and hydrometeorology. J Clim Appl Meteorol 23:201–213